Large-Scale Simultaneous Orientation of CdSe Nanorods and Regioregular Poly(3-hexylthiophene) by Mechanical Rubbing

ARTICLE *in* MACROMOLECULES · AUGUST 2013

Impact Factor: 5.8 · DOI: 10.1021/ma400880x

Macromolecules

Article

pubs.acs.org/Macromolecules

Large-Scale Simultaneous Orientation of CdSe Nanorods and Regioregular Poly(3-hexylthiophene) by Mechanical Rubbing

Lucia Hartmann,[†,‡,#] David Djurado,[‡] Ileana Florea,[§] Jean-François Legrand,[†] Angela Fiore,[‡] Peter Reiss,[‡] Stephen Doyle,[∥] Alexeï Vorobiev,[⊥] Stéphanie Pouget,[‡] Frédéric Chandezon,[‡] Ovidiu Ersen,[§] and Martin Brinkmann*[,†]

[†]ICS (UPR22-CNRS), 23 rue du Loess, BP 84047, 67034 Strasbourg Cedex 2, France

[‡]UMR SPrAM 5819 (CEA-CNRS-UJF) and SP2M, CEA Grenoble/INAC, 38054 Grenoble Cedex, France

[§]IPCMS (UMR 7504 CNRS − Université de Strasbourg), 23 rue du Loess, BP 43, 67034 Strasbourg Cedex 2, France

[∥]Institut für Synchrotronstrahlung (ISS), Hermann-von-Helmholtz-Platz 1, D-76344 Eggenstein-Leopoldshafen, Germany

[⊥]ESRF, 6 rue J. Horovitz, BP220, 38043 Grenoble Cedex 9, France

Supporting Information

ABSTRACT: Highly oriented hybrid thin films composed of rod-shaped CdSe nanocrystals and poly(3-hexylthiophene) are prepared by mechanical rubbing. The orientation distribution of both CdSe nanorods and crystalline P3HT domains is determined by a combination of transmission electron microscopy (electron diffraction, low dose high-resolution TEM, and tomography), grazing incidence X-ray diffraction measurements, and UV−vis spectroscopy. After rubbing, P3HT crystalline domains show a preferential face-on orientation ((010) contact plane) and the chains align parallel to the rubbing direction. CdSe nanorods also align parallel to the rubbing direction, but the level of alignment is a function of their concentration in the polymer matrix: the lower their concentration, the higher the level of in-plane orientation of both the nanorods and the polymer chains. GIXD and electron diffraction suggest that CdSe nanorods adopt a preferential contact plane on the substrate after rubbing. The high in-plane alignment of the nanorods is mainly due to the orientation of the surrounding P3HT matrix. In particular, low dose HR-TEM shows that the local orientation of individual NRs matches the orientation of the surrounding π-stacked P3HT chains. For a high NR concentration, bundling of NRs into larger aggregates prevents their efficient alignment by rubbing.

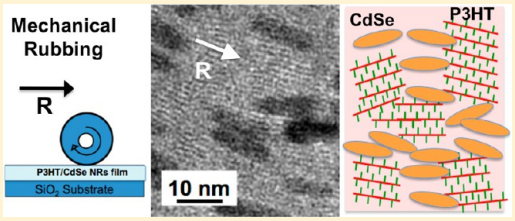

I. INTRODUCTION

Functional hybrid materials composed of conjugated polymers such as regioregular poly(3-alkylthiophene)s (P3AT) and semiconductor quantum dots, e.g. CdSe, has gained increasing interest in the field of plastic electronics during the past years.[1−7] This interest is mainly due to the possibility of combining the facile solution processing of semiconducting polymers such as poly(3-hexylthiophene) (P3HT) with the tunable electronic properties and high environmental stability of semiconducting nanocrystals. Therefore, this type of hybrid materials is particularly appealing for use in organic solar cells, photodetectors, and field effect transistors.[1−7]

As compared to nanospheres, hybrid thin films containing rod-shaped nanocrystals have shown improved charge transport and/or polarized optical properties.[1,4,7] For the elaboration of efficient electroactive layers in devices, the control of the orientation of the nanorods (NRs) and the polymer chains is essential since charge transport in both CdSe NRs and semiconducting polymers like P3HT is highly anisotropic.[8] It is therefore of importance to find new and simple orientation methods to prepare hybrid films made of both oriented polymer chains and NRs, especially in view of the fabrication of ambipolar field effect transistors.[2] The controlled orientation of the NRs over large surfaces remains still a challenge although some progress has been made by using self-assembly or the application of external fields (electric, magnetic).[9−15] For instance, alignment of CdSe nanorods perpendicular to the substrate plane was realized by controlled solvent evaporation or by application of an external electric field.[16−20] Thin films of pure NRs were aligned by mechanical rubbing with a velvet cloth leading to partial in-plane alignment of the nanorods parallel to the rubbing direction.[21−24] Stretching of polymers such as polyethylene or poly(vinyl alcohol) containing rod-shaped colloidal nanocrystals was reported to yield uniaxially aligned NRs within the stretched polymer matrix.[22,25−28] Template patterns such as for example PDMS were also used to orient NRs and prepare devices.[29,30]

At the same time, the orientation and the control of the morphology of conjugated polymers and in particular of P3HT have also seen significant progress.[8,31−33] However, the simultaneous orientation of both NRs and the polymer in hybrid materials is more difficult to achieve and has only

Received: April 30, 2013
Revised: June 25, 2013
Published: July 16, 2013

recently been obtained by means of directional epitaxial crystallization.[34] In most other reported studies, either the polymer matrix or the nanoparticles are well oriented, but not both. As an example, Schierhorn et al. realized hybrid materials composed of a regular pattern of vertically aligned CdSe NRs that was subsequently impregnated with P3HT, but neither the CdSe NRs nor the P3HT polymer was showing any preferential crystalline orientation.[35] Gupta et al. realized vertically aligned NR within a P3HT matrix by applying an electric field, but the P3HT was not oriented.[20] Snaith et al. reported hybrid films composed of oriented polyacrylate and nonoriented nanocrystals.[36] However, to the best of our knowledge, little has been reported about hybrid systems composed of conjugated polymers and inorganic nanorods where both components are oriented. Here, we report the fabrication of oriented hybrids composed of CdSe NRs and P3HT, where both the NRs and the P3HT matrix show a high in-plane orientation. We demonstrate that mechanical rubbing of hybrid thin films is a simple and efficient method for the fabrication of large surfaces of oriented hybrid thin films. This method is an attractive alternative to directional epitaxial crystallization, a method based on the slow directional growth of a polymer in a temperature gradient in the presence of a suitable crystallizable solvent.[8] Rubbing of polymers is well established in the field of display technology which makes use of polymer alignment layers, e.g., polyimides.[37,38] Rubbing of polyimide films leads to near-surface alignment of the polymer chains that helps orienting liquid crystal molecules or polymers. Recently, mechanical rubbing has been successfully used to orient conjugated polymers, e.g. P3HT, leading to highly oriented films with anisotropic charge transport properties.[8] The level of orientation achieved in the thin films was shown to depend strongly on the molecular weight of the polymer.[8]

The present study first focuses on the orientation distribution of both crystalline P3HT domains and CdSe NRs in the rubbed thin films as investigated by transmission electron microscopy (low dose HR-TEM and electron diffraction), UV−vis spectroscopy, and grazing incidence X-ray diffraction measurements (GIXD). Second, the impact of the NR concentration on the ultimate in-plane orientation level is investigated, and the orienting character of the polymer matrix on the CdSe NRs is demonstrated.

II. EXPERIMENTAL SECTION

1. Materials. The P3HT sample used in this study was purchased from Merck and characterized by gel permeation chromatography (M_w = 17.6 kDa, M_n = 13.4 kDa, PDI = 1.3).

CdSe nanorods (20 nm × 5 nm) were synthesized following the so-called seeded-growth approach originally developed to obtain rod-shaped nano-heterostructures.[39,40] Octadecylphosphonic (ODPA), hexylphosphonic (HPA), and tetradecylphosphonic acids (TDPA) were purchased from Polycarbon Industries. Trioctylphosphine (TOP, 90%) and trioctylphosphine oxide (TOPO, 99%) were purchased from Aldrich. All reagents were used as received. Spherical CdSe nanocrystals (ϕ = 3−4 nm) are first synthesized and purified. Then, they are coinjected with TOPSe solution to the reaction mixture that contains the solvent, surfactants, and the cadmium precursor to serve as seeds for the growth of the CdSe NRs. For the CdSe NRs of dimensions 20 nm × 5 nm used in this study (see Figure S0), seeds of 3 nm diameter were used. For the synthesis of the seeds, TOPO (3.0 g), TDPA (234 mg), and CdO (60 mg) are mixed in a 50 mL flask heated to ca. 150 °C and degassed under vacuum during 1 h. The flask is then heated to 300 °C under a nitrogen flow until the solution turns optically clear and colorless. At this point, 1.5 g of TOP is injected into the flask, the temperature is raised to 350 °C, and then a TOPSe solution (58 mg of Se mixed with 360 mg of TOP) is swiftly injected. The heating mantle is removed afterward, and the spherical CdSe seeds are recovered by a repeated precipitation with addition of methanol and redispersion in toluene. The seed solution used for the growth of the NRs is obtained by adding 1.7 nmol of the synthesized CdSe nanospheres to 1 mL of TOP and 19 mg of Se. The amount of seeds is obtained from absorption measurements.[40] In a 50 mL flask, 60 mg of CdO is blended with TOPO (3 g), ODPA (280 mg), and HPA (80 mg). After pumping the flask for ca. 1 h at 150 °C, the resulting solution is heated under a nitrogen flow to 300 °C. At this step, 1.5 g of TOP is injected, and when the temperature of the solution has been stabilized at 300 °C, the seed solution is swiftly injected into the flask. The NRs are allowed to grow for 7 min, after which the heating mantle is removed. Then the NRs are recovered using the standard procedure of precipitation with addition of methanol and redispersion in toluene.

Hybrid films are prepared from the corresponding blend solutions by doctor blading using a homemade apparatus onto precleaned glass slides or Si(100) substrates at 35 °C. The P3HT/CdSe NRs blend solutions are prepared by mixing a 8 wt % P3HT solution in chlorobenzene and a corresponding solution of CdSe NRs in toluene. Both solutions were kept for 1 h at 40 °C and then filtered with a poly(tetrafluoroethylene) filter (200 μm) before mixing. The cleaning of the glass substrates is described in ref 38a. In the following, the relative composition of the CdSe NRs in the films is given in wt % according to the ratio P3HT:CdSe. The thickness of the films probed by TEM tomography is in the range 30−60 nm.

Orientation of the films by mechanical rubbing follows the procedure described in our earlier work for the preparation of polycarbonate alignment layers.[38a−e] It involves mainly two steps: (i) the preparation of a hybrid film by the doctor blade method and (ii) rubbing of the as-deposited films with a microfiber tissue. The rubbing machine is composed of a rotating cylinder (4 cm diameter) covered by a microfiber cloth. The rubbing is performed by applying the rotating cylinder with a 2 bar pressure on the translating sample holder. Each cycle of rubbing is characterized by a 50 cm rubbing length, i.e., the length of the rubbing tissue applied on a given point of the sample. The highest orientation is usually observed after 3−4 rubbing cycles.

2. Characterization of the Oriented Hybrid Layers. *TEM*: Oriented areas were first identified for TEM analysis by optical microscopy (Leica DMR-X microscope). The P3HT/CdSe-NRs films were coated with a thin amorphous carbon film, and the carbon-coated film was removed from the SiO_2 substrate by using poly(acrylic acid) (25% aqueous solution, Aldrich) and subsequently recovered onto TEM copper grids. TEM was performed in bright field, high resolution, dark field and diffraction modes using a CM12 Philips microscope equipped with a MVIII (Soft Imaging System) charge coupled device camera. Calculation of the fiber pattern for CdSe nanocrystals was realized using the diffraction module of the Cerius^2 software (Accelrys).

TEM Tomography: Experimental data for tomography were acquired by means of a spherical aberration (Cs) probe corrected JEOL 2100F transmission electron microscope with a field emission gun operating at 200 kV. The tilt series of BF images were recorded with a 2048 × 2048 pixel cooled CCD detector having a pixel size of about 0.2 nm and a 1 s exposure time for each record. The angular range sampled during the acquisition was between +70° and −70°, with a tilt increment given by a 2° Saxton scheme,[41] giving a total of 90 images. Once the acquisition of the tilt series was completed, the images were first roughly aligned using a cross-correlation algorithm. A refinement of this initial alignment was then obtained with the IMOD software[42] using the positions of the nanoparticles as fiducial markers. The volumes reconstructions were computed using algebraic reconstruction techniques (ART) implemented in the TomoJ software[43] with a number of iterations not exceeding 20. Considering the acquisition parameters and the characteristics of the specimen under study, the relations from Midgley et al.[44] provide a spatial resolution of about 1.5 nm in the plane perpendicular to the electron beam. In the parallel direction, the resolution is worsened by a factor

dx.doi.org/10.1021/ma400880x | Macromolecules 2013, 46, 6177−6186

of 1.1 due to the limited maximum tilt angle. To model the calculated volume, a segmentation procedure based on the gray-level intensities of the voxels, followed by a classical surface rendering process, were systematically used. More details on the experimental setup, volume reconstruction, and analysis can be found elsewhere.[45] Visualization and quantitative analysis of the final volumes were carried out using Slicer 3.5 and ImageJ softwares.

GIXD measurements were performed with a linear and a 2D detector at the ESRF on the beamline ID10b at a wavelength $\lambda = 0.59$ Å and at ANKA on the PDIFF line with $\lambda = 1.24$ Å with incidence angles of 0.06° and 0.15°, respectively. For P3HT, the critical angles for X-rays at 0.59 and 1.24 Å are 0.065° and 0.136°, respectively. Given the oriented character of the films, two geometrical scattering configurations are used: $\mathbf{q}_i \| \mathbf{R}$ and $\mathbf{q}_i \perp \mathbf{R}$, with $\mathbf{q}_i$ the $\mathbf{q}$ vector of the incident X-ray beam and $\mathbf{R}$ the rubbing direction (see schematic illustration in Figure 1 and 4). The out-of-plane scattering vector is

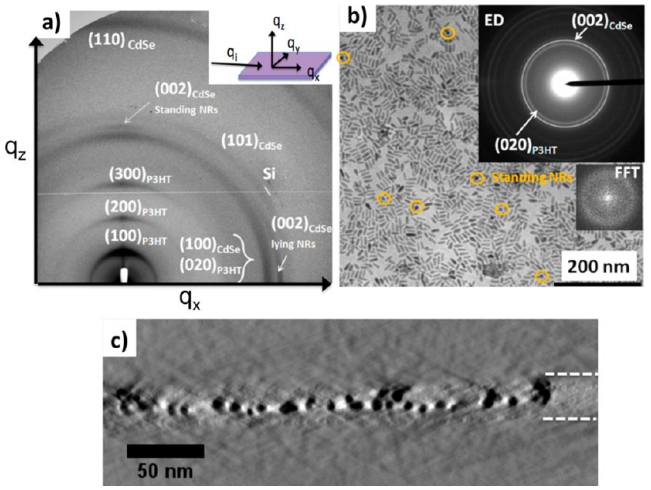

Figure 1. (a) 2D GIXD map and (b) TEM-BF and corresponding ED pattern of an as deposited hybrid thin film with a composition of P3HT:CdSe 1:1 in wt %. The inset shows the FFT of the TEM-BF image. The yellow circles evidence some standing rods (with their long axis perpendicular to the plane of underlying substrate). (c) Cross-sectional slice as obtained from a tomographic analysis of the 3D morphology of the hybrid layer. The two dotted lines highlight the boundaries of the P3HT matrix. The substrate/film interface is on the upper side of the cross-section slice.

labeled $\mathbf{q}_z$. We have also performed so-called omega (Ω) scans around specific reflections (mainly $(100)_{P3HT}$) in order to quantify the in-plane orientation distribution of the crystals. $\Omega = 0°$ corresponds to $\mathbf{q}_i \| \mathbf{R}$ and $\Omega = 90°$ to $\mathbf{q}_i \perp \mathbf{R}$.

The level of orientation of rubbed hybrid thin films was also evaluated by UV−vis absorption spectroscopy using a Shimadzu UV-2101PC spectrometer (spectral resolution of 1 nm) and polarized incident light. The orientation of the film with respect to the polarization of the incident beam is controlled by a goniometer. The parallel configuration is such that the incident light polarization is parallel to the $\mathbf{c}_{P3HT}$ axis (rubbing direction $\mathbf{R}$).

III. RESULTS AND DISCUSSION

1. As-Deposited Hybrid CdSe/P3HT Films. In order to precisely evaluate the impact of mechanical rubbing on the orientation of P3HT:CdSe thin films (1:1 in wt %), a first characterization of the as-deposited hybrid layers prepared by the doctor blade method has been performed using both TEM and GIXD measurements. Figure 1 shows the TEM-BF image, the corresponding ED pattern, and a 2D GIXD map of an as-deposited P3HT/CdSe film.

The TEM-BF image shows that the NRs are rather well dispersed and not aggregated although some fluctuations in NR density are observed over the film surface. NRs are oriented in majority with their long axis lying in-plane with only a few standing rods. This is further confirmed by a tomographic analysis of the films. The cross-sectional slice obtained by TEM tomography, i.e., without cutting the sample (Figure 1c), shows that the CdSe NRs are lying in the plane of the substrate and are embedded in the P3HT matrix without segregation at the film/substrate or air/film interfaces. No preferential in-plane orientation of the long axis of these NRs is observed, as confirmed by the ED pattern where the $(002)_{CdSe}$ reflection of the NRs shows a uniform Scherrer ring characteristic of a 2D powder. GIXD confirms that most of the rods are lying parallel to the substrate as the $(002)_{CdSe}$ appears essentially in the in-plane ($\mathbf{q}_x$) direction with a small fraction of standing rods as identified by the corresponding $(002)_{CdSe}$ reflection along $\mathbf{q}_z$. The 2D GIXD map shows the $(h00)_{P3HT}$ reflections mainly along the $\mathbf{q}_z$ direction although some much weaker in-plane contribution can be distinguished. This is the fingerprint of a preferential "edge-on" orientation ($\mathbf{a}_{P3HT}$* perpendicular to the substrate) of the P3HT crystalline domains with a small amount of powder-like distributed domains. This is identical to what was observed in a previous work for doctor-bladed P3HT films.[8] The ED pattern showing the π-stacking (020) reflection of the P3HT as a continuous Scherrer ring indicates no preferential in-plane orientation of the P3HT crystalline domains.

2. Structure and Morphology of Hybrid Thin Films (1:1 in wt %) after Rubbing. In contrast to most reported works on the alignment of nanorods by mechanical rubbing,[20−22] we were interested in the fabrication of hybrid thin films where both the NRs and the polymer (P3HT) are highly oriented. In our previous work on rubbing of pure P3HT, it was shown that rubbing of P3HT results in (i) an alignment of the chain axis $\mathbf{c}_{P3HT}$ parallel to the rubbing direction $\mathbf{R}$ and (ii) a change of the P3HT nanocrystal's orientation from an initial "edge-on" to a final "face-on" ($\mathbf{b}_{P3HT}$ perpendicular to the substrate) orientation of the conjugated P3HT chains after rubbing.[8]

Figures 2a and 2b show the TEM-BF image of a rubbed 1:1 hybrid thin film and the corresponding ED pattern, respectively. The BF image reveals a preferential alignment of all NRs along the rubbing direction. The obtained alignment of the hybrid film and in particular the CdSe NRs is improved and more uniform with respect to that obtained by rubbing pure CdSe films (see Figure S1). The ED pattern in Figure 2b shows characteristic reflections of both the oriented P3HT matrix and the aligned NRs albeit the reflections of CdSe NRs are dominant because of their stronger scattering ability as compared to P3HT. On the meridian of the ED pattern, an intense and arced reflection corresponding to the $(002)_{CdSe}$ planes of CdSe is observed. Dark field imaging (Figure S2) confirms the identification of this reflection. As seen in Figure S2, the dark field image displays exclusively the CdSe nanorods in bright whereas the nondiffracting P3HT matrix remains dark. Several reflections are present on the equator of the ED pattern. They are associated with both P3HT crystallites and CdSe NRs. The sequence of $(h00)_{P3HT}$ reflections ($h = 1-3$) characteristic of the oriented P3HT is observed, as well as two broad reflections attributed to $(100)_{CdSe}$ and $(110)_{CdSe}$. This ED pattern indicates that both the CdSe NRs and the P3HT domains show a well-defined preferential in-plane orientation,

dx.doi.org/10.1021/ma400880x | Macromolecules 2013, 46, 6177−6186

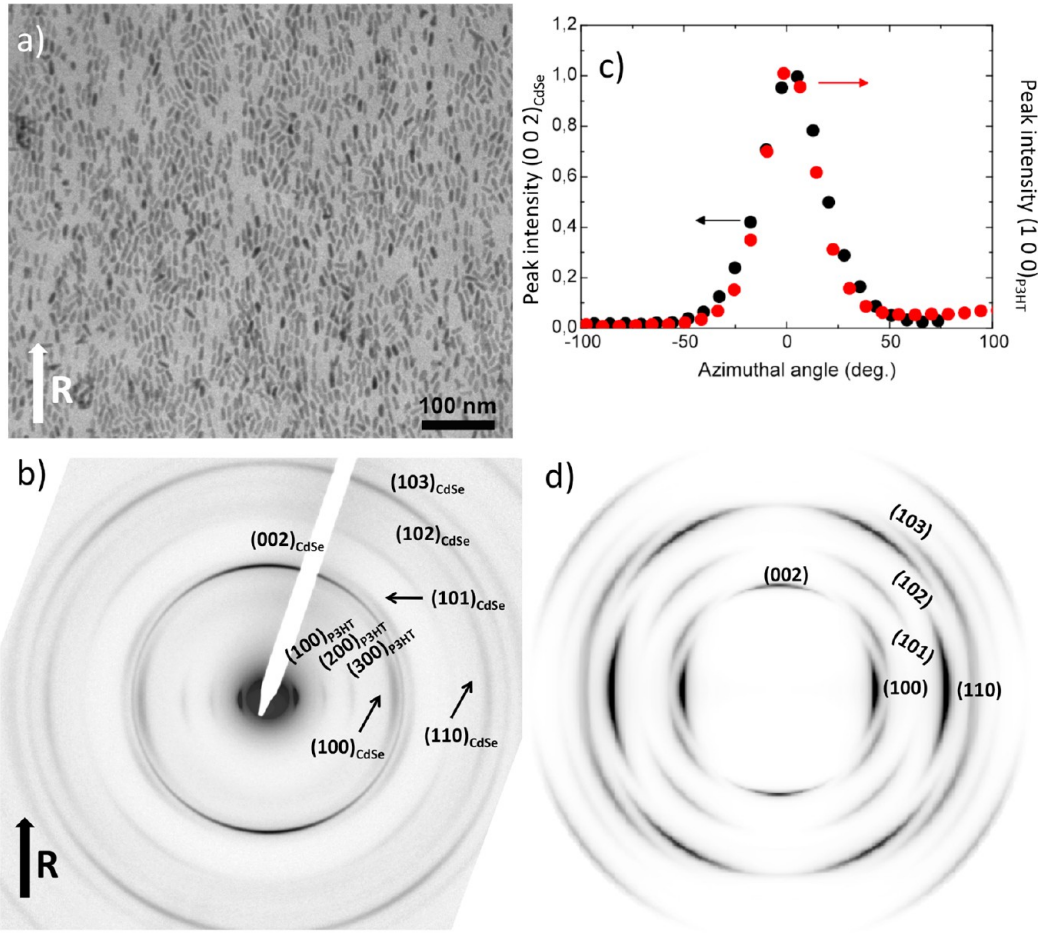

Figure 2. (a) TEM-BF image of a rubbed sample with a composition 1:1 and (b) corresponding ED pattern in proper relative orientation. (c) Azimuthal intensity peak profile of the $(100)_{P3HT}$ and the $(002)_{CdSe}$ reflections. (d) Calculated fiber pattern of CdSe for an azimuthal in-plane distribution characterized by a fwhm ∼ 15°.

i.e., $\mathbf{c}_{P3HT}\|\mathbf{R}$ and $\mathbf{c}_{CdSe}\|\mathbf{R}$. The presence of the $(h00)_{P3HT}$ reflections and the absence of the π-stacking reflection of P3HT on the equator of the ED pattern indicate that the crystalline domains of P3HT changed their preferential orientation on the Si(100) substrate from the "edge-on" to the "face-on" orientation as already observed with pure P3HT layers upon rubbing.[8] This high in-plane orientation of the polymer leads to a corresponding anisotropy of the UV−vis absorption as shown in Figure S3 with a characteristic dichroic ratio at 600 nm in the range 3.5−4.0 similar to that obtained for rubbed 20 kDa P3HT films.[8] It must be stressed that the determination by UV−vis absorption of the P3HT orientation using the dichroic ratio at 600 nm is hampered by the presence of the overlaping CdSe contribution. The same holds true for the determination of orientation of CdSe NRs in the P3HT matrix using photoluminescence measurements. Therefore, the quantitative determination of the in-plane orientations of both P3HT and CdSe NRs via GIXD and ED is more robust.

TEM tomography was further used to characterize the 3D morphology of the rubbed films. TEM tomography allows reconstructing the 3D distribution of CdSe NRs in the polymer matrix avoiding the damaging of the layers caused by microtoming thin slices of the material.[46] Figure 3 shows the characteristic tomographic views of a P3HT/CdSe hybrid layer (1:1 in wt %) after rubbing. As seen in Figure 3c, besides a few aggregates of largely unoriented CdSe NRs, most NRs are located close to the film/substrate interface, whereas in the as-deposited film, the CdSe NRs are distributed more in the interior of the film (see Figure 1c). This observation indicates that besides the in-plane orientation of CdSe NRs parallel to the rubbing direction, an internal redistribution of CdSe NRs in the bulk of the P3HT film occurs: rubbing tends to push the NRs down to the interface with the substrate (glass) through the P3HT matrix. This result indicates that the P3HT film shows a plastic deformation upon shearing during mechanical rubbing with a redistribution of material inside the film.

2. In-Plane and Out-of-Plane Orientation of the Polymer and NRs As Probed by GIXD Measurements. GIXD measurements with a 2D detector were performed to obtain statistical information on the NRs orientation both in- and out-of-plane over an approximately 1 cm^2 sample area. Figure 4 shows the GIXD 2D maps of the hybrid thin film for the incidence X-ray beam oriented parallel (Ω = 0°) and perpendicular (Ω = 90°) to the rubbing direction **R** (the sample is rotated around the film normal, i.e., the $\mathbf{q}_z$ direction). The rocking curves for the $(002)_{CdSe}$ reflection for hybrid layers with different CdSe concentrations (see Figure 5) were obtained from in-plane GIXD 1D scans using a point detector and a Bragg geometry. In the Bragg configuration, for Ω = 0° the scattering vector **q** is perpendicular to the rubbing direction **R**, i.e. $\mathbf{q}\perp\mathbf{R}$, whereas for Ω = 90°, $\mathbf{q}\|\mathbf{R}$. All GIXD patterns

dx.doi.org/10.1021/ma400880x | Macromolecules 2013, 46, 6177−6186

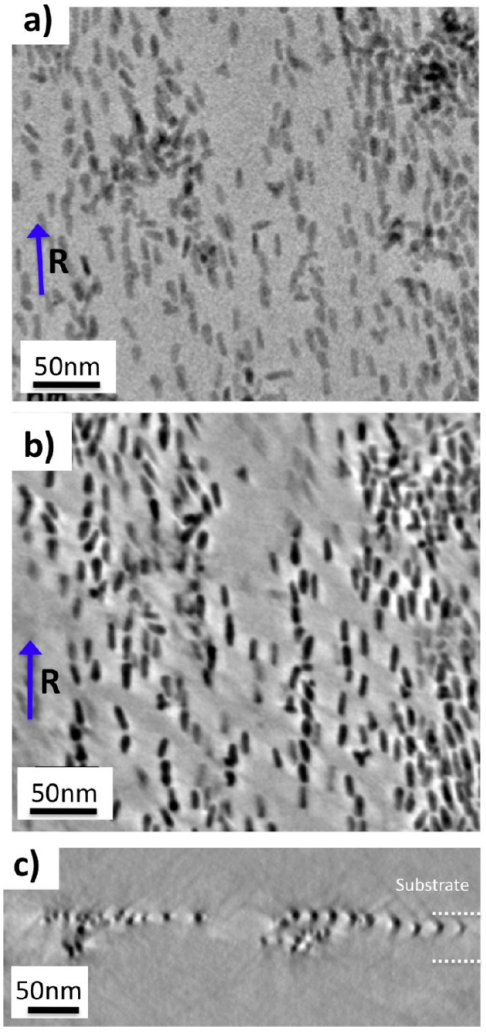

Figure 3. (a) Conventional TEM 2D view of a 1:1 P3HT/CdSe NR film. (b) Longitudinal slice in the plane of the thin film. (c) Transversal (cross-sectional) slice. The upper and lower interfaces of the hybrid layer are highlighted by two dotted lines. The substrate/film interface is on the upper side of the cross section views as indicated.

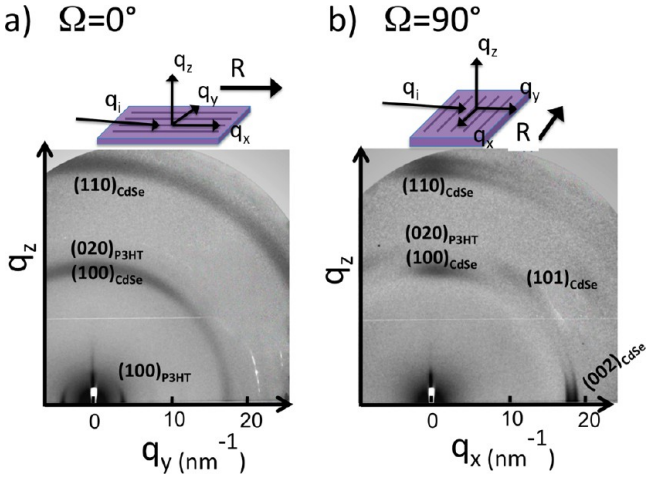

Figure 4. 2D GIXD intensity maps of a rubbed P3HT/CdSe sample with a composition of 1:1 in weight. (a) Ω = 0° corresponds to the configuration $\mathbf{q}_i \| \mathbf{R}$ and (b) Ω = 90° corresponds to $\mathbf{q}_i \perp \mathbf{R}$ ($\mathbf{q}_i$ the vector of the incident X-ray beam).

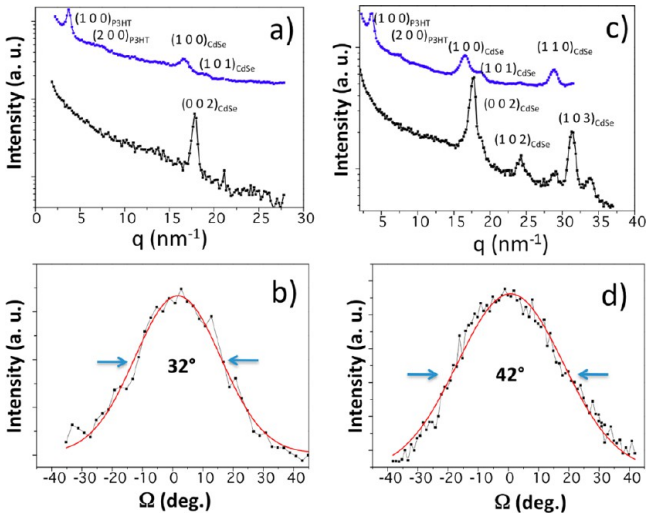

Figure 5. GIXD linear scans recorded with the incident scattering vector $\mathbf{q}_i$ parallel (blue top curve) and perpendicular (black bottom curve) to the rubbing direction and corresponding in-plane rocking curves of the $(002)_{CdSe}$ reflection for rubbed P3HT/CdSe thin films with a composition in weight of 1:1 (a, b) and 1:3 (c, d).

exhibit characteristic reflections of both oriented P3HT and CdSe NRs.

Let us first consider the orientation of the polymer matrix. As seen in Figure 4, for Ω = 0°, one dominant in-plane reflection corresponding to $(100)_{P3HT}$ is seen and one $(020)_{P3HT}$ reflection in the $\mathbf{q}_z$ direction. The latter reflection overlaps presumably with the intense $(100)_{CdSe}$ reflection. For Ω = 90°, only the $(020)_{P3HT}$ reflection corresponding to the π-stacking direction is observed along $\mathbf{q}_z$.

The linear scans recorded in Bragg geometry for the 1:1 hybrid layer are shown in Figure 5a for $\mathbf{q}_i \| \mathbf{R}$ and $\mathbf{q}_i \perp \mathbf{R}$. As expected for a high in-plane orientation of the P3HT domains with a "face-on" orientation of chains, only the characteristic $(h00)_{P3HT}$ reflections are visible for $\mathbf{q}_i \| \mathbf{R}$. Altogether, these observations indicate that (i) the P3HT chains are oriented parallel to the rubbing **R** and (ii) the initially edge-on oriented P3HT domains have adopted a preferential "face-on" orientation after rubbing.[8] These observations are consistent with the TEM results, suggesting that the orientation process of the P3HT matrix is qualitatively not modified by the presence of CdSe NRs.

Considering the orientation of CdSe NRs, the 2D GIXD map (Figure 4a) for Ω = 0° shows two characteristic Scherrer rings: they correspond to $(100)_{CdSe}$ and $(110)_{CdSe}$ diffracting planes of the CdSe NRs. A uniform intensity distribution of the Scherrer ring would indicate a fiber-like distribution of the CdSe NRs with their long axis (*c*-axis) oriented along the rubbing direction. However, the intensity of the $(100)_{CdSe}$ reflection is not uniform; it is clearly stronger along the $\mathbf{q}_z$ direction. This suggests that the CdSe NRs do not show a pure fiber-like distribution of their orientation with the $\mathbf{c}_{CdSe}$ axis parallel to the rubbing direction **R**, but some preferential contact plane of the NRs is probably present. Preferential contact planes of the NRs were also observed in the case of rubbed CdSe NR films deposited on PEDOT:PSS substrates with a preferential alignment $\mathbf{c}_{CdSe} \| \mathbf{R}$ and the *a*−*c* (or, equivalently, *b*−*c*) plane of CdSe NRs lying parallel to the substrate plane.[21] This point will be further demonstrated by the analysis of the ED pattern (vide infra).

dx.doi.org/10.1021/ma400880x | *Macromolecules* 2013, 46, 6177−6186

For Ω = 90° (Figure 4b), the $(100)_{CdSe}$ and $(110)_{CdSe}$ reflections are strongly narrowed along $\mathbf{q}_z$, while the sharp $(002)_{CdSe}$ is observed on the equator. Of particular interest is the fact that the rubbed hybrid layers do not show any trace of the $(0\ 02)_{CdSe}$ reflection in the $\mathbf{q}_z$ direction, contrary to the as-deposited films prior to rubbing (see Figure 2). This indicates that the few rods initially "standing up" have all been oriented in the plane of the film after rubbing. This is also consistent with the TEM results showing essentially lying CdSe NRs.

Using the electron diffraction data and the linear Ω scans, the in-plane angular distributions of the NR's orientations was determined for the 1:1 sample. Both electron diffraction and GIXD yielded a similar value of 32° for the full width at half-maximum (fwhm) of the $(002)_{CdSe}$ peak. The good agreement of the results from ED and GIXD measurements shows that the orientation distribution inferred from the ED pattern over ~100 μm^2 area of the hybrid films is representative of the in-plane distribution observed over the entire film surface by GIXD (in the range of 1 cm^2). This result demonstrates that the rubbing method achieves a very uniform in-plane alignment of both the polymer and the CdSe NRs over surfaces as large as a few cm^2. The comparison with the literature shows that the hybrid CdSe/P3HT films are better oriented than rubbed films of pure CdSe NRs.[21] In rubbed thin films of CdSe nanorods on a PEDOT:PSS substrate, the in-plane and the out-of-plane orientations of the NRs are characterized by typical fwhm of 52° and 18°, respectively.[21] Clearly, the in-plane alignment of CdSe NRs is significantly improved in the hybrid layers comparatively to rubbed films of pure CdSe NRs. This result underlines the important role of the polymer matrix on the alignment mechanism of the CdSe NRs.

4. Preferential Orientation of CdSe NRs in the Rubbed Hybrid Films. In order to analyze more carefully the composite ED pattern of the rubbed films, one fiber diffraction pattern of CdSe has been calculated using the Cerius^2 program and is displayed in Figure 2d. It was obtained by taking into account the dimensions of the CdSe NRs with an orientation distribution around the fiber axis of 15° full width at half-maximum (fwhm). The calculated ED fiber pattern accounts well for the presence of all reflections of CdSe NRs in the hybrid layers (see Figure 2b). However, a careful analysis reveals a few remarkable differences in terms of relative intensities of the reflections. In the case of the calculated fiber pattern, the $(100)_{CdSe}$ and the $(103)_{CdSe}$ reflections are the most intense ones. However, in the experimental ED pattern, the $(002)_{CdSe}$ reflection is the most intense one, whereas the intensity of the equatorial $(100)_{CdSe}$ and $(110)_{CdSe}$ reflections is lower than expected from the calculated fiber pattern. This observation is consistent with the GIXD results showing a nonuniform intensity distribution of the $(100)_{CdSe}$ reflection with a higher intensity along the film normal direction ($\mathbf{q}_z$). Taken altogether, these results suggest that CdSe nanorods adopt some preferential contact planes on the substrate after rubbing. A possible origin for preferential contact planes of CdSe NRs might be the faceting of the nanocrystal's "lateral" surface as evidenced by Z-STEM.[47]

5. Origin of the In-Plane Alignment of CdSe NRs. The fact that both the CdSe NRs and the crystalline P3HT domains are oriented by the rubbing is particularly interesting from the point of view of charge transport as the direction of facile transport in the nanorods and the polymer are parallel to the rubbing direction. Moreover, it has been shown that, for P3HT alone, transport is strongly improved along the rubbing direction comparatively to the perpendicular direction.[8] Regarding the orientation of the CdSe NRs in the rubbed hybrid films, it may be induced in two manners: (i) by direct orientation enforced by the microfiber tissue (as in the case of rubbed films of pure CdSe NRs) and/or (ii) indirectly via the orientation of the P3HT polymer matrix. In the latter case, one would expect a correlation between the in-plane orientation of the P3HT domains and the CdSe NRs. To verify this last possibility, the in-plane intensity distributions of both $(100)_{P3HT}$ and $(002)_{CdSe}$ diffraction peaks were extracted from the ED pattern in Figure 2b, and the resulting curves are shown in Figure 2c. As seen in Figure 2c, the two azimuthal distributions are almost overlapping and are both characterized by a full width at half-maximum (fwhm) of approximately 32°. This result supports the fact that it is the orientation of the P3HT matrix that enforces the in-plane orientation of the NRs since the observed NR in-plane orientation is significantly better in the hybrid layers as compared to films of NRs alone (fwhm ~ 45°−50°; see Supporting Information). To further visualize the correlation between the orientation of the NRs and the P3HT chain orientation, we performed low dose HR-TEM observations of the hybrid layers. In fact, HR-TEM gives directly access to the crystalline domains and to the chain packing in a 2D projection in contrast to other indirect methods such as X-ray diffraction. Indeed, in our recent reports, the stacks of adjacent P3HT chains in face-on orientation on a substrate were clearly observed by HR-TEM.[48] Figure 6 shows

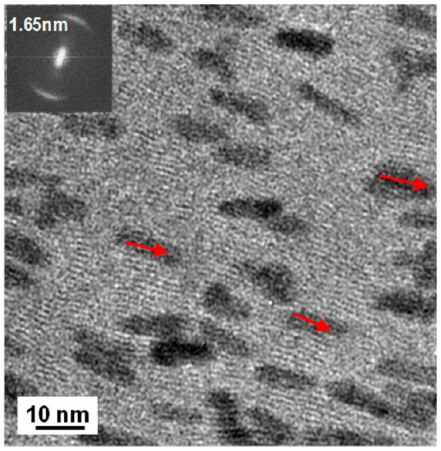

Figure 6. HR-TEM image of a rubbed hybrid thin film with a composition 2:1. The inset shows the FFT with the periodicity along the $\mathbf{a}_{P3HT}$-axis of the P3HT. Red arrows show the orientation of CdSe long axis.

a representative HR-TEM image obtained for a rubbed hybrid film with a composition P3HT:CdSe 2:1. Fringed patterns with a 1.65 nm periodicity are clearly observed between the darker CdSe NRs. These fringed patterns correspond to planes of π-stacked chains separated by the hexyl side chains ($\mathbf{a}_{P3HT}$ = 1.65 nm periodicity). In HR-TEM, the "face on" oriented stacks of P3HT chains are clearly observed because of the Z contrast between the sulfur-rich stacks of polythiophene backbones and the layers of *n*-hexyl side chains. Most interestingly, Figure 6 shows that the local orientation of the NRs follows that of the adjacent P3HT polymer stacks. This effect is illustrated by red arrows on the HR-TEM image. This observation gives further support for the fact that the alignment of the CdSe NRs is due to a large extent to the alignment of the surrounding P3HT

dx.doi.org/10.1021/ma400880x | Macromolecules 2013, 46, 6177−6186

matrix. This point is further demonstrated by following the level of in-plane alignment as a function of the NP content in the hybrid thin films as detailed in the next section.

6. Effect of NR Concentration on the In-Plane Orientation after Rubbing. Figure 7 shows the TEM-BF and the corresponding ED patterns of hybrid samples of various P3HT:NRs compositions. The TEM-BF shows some fluctuations in the density of NRs in the P3HT matrix at the length scale of several micrometers but no macrophase separation. The NRs tend to align parallel to the rubbing direction ($\mathbf{c}_{CdSe}\|\mathbf{R}$) in all hybrid films. The 1:1 sample shows linear rail-track assemblies of CdSe NRs oriented along the rubbing direction, whereas for higher CdSe NR concentrations, bundling of the NRs into small raft-like aggregates is observed and in-plane alignment tends therefore to decrease. The decrease of in-plane alignment of CdSe NRs with increasing concentration of NRs is further manifested by the evolution of the angular spread of the $(002)_{CdSe}$ in the ED patterns of Figure 7. The full width at half-maximum (fwhm) of the azimuthal distributions of the $(002)_{CdSe}$ and $(100)_{P3HT}$ reflections were extracted from the ED patterns. In addition, Ω-scans were also recorded by GIXD for the 1:3 sample (Figure 5d). The results obtained by ED on a relatively small scale match well the results obtained by GIXD on the cm^2 scale. This confirms that the information obtained by TEM is representative of the entire sample. Samples characterized by a ratio P3HT:CdSe up to 1:2 show similar in-plane distributions of both P3HT chains and CdSe nanorods with a typical fwhm of 32°−35°. For the 1:3 sample, the in-plane orientation of the NRs is characterized by a fwhm of 42° for the $(002)_{CdSe}$ reflection. This value is lower albeit close to that obtained for rubbed CdSe NRs films, i.e., 46°. For all investigated sample compositions, a close matching of both the angular distributions of the $(100)_{P3HT}$ and the $(002)_{CdSe}$ was observed, underlining the strong correlation between the polymer chain and CdSe NRs orientation in the hybrid layers. In addition, the evolution of the fwhm of the $(002)_{CdSe}$ peak obtained by ED and GIXD versus CdSe concentration (see Figure 8) reveals a clear trend: the overall in-plane alignment of CdSe NRs and polymer chains decreases with increasing concentration of CdSe NRs.

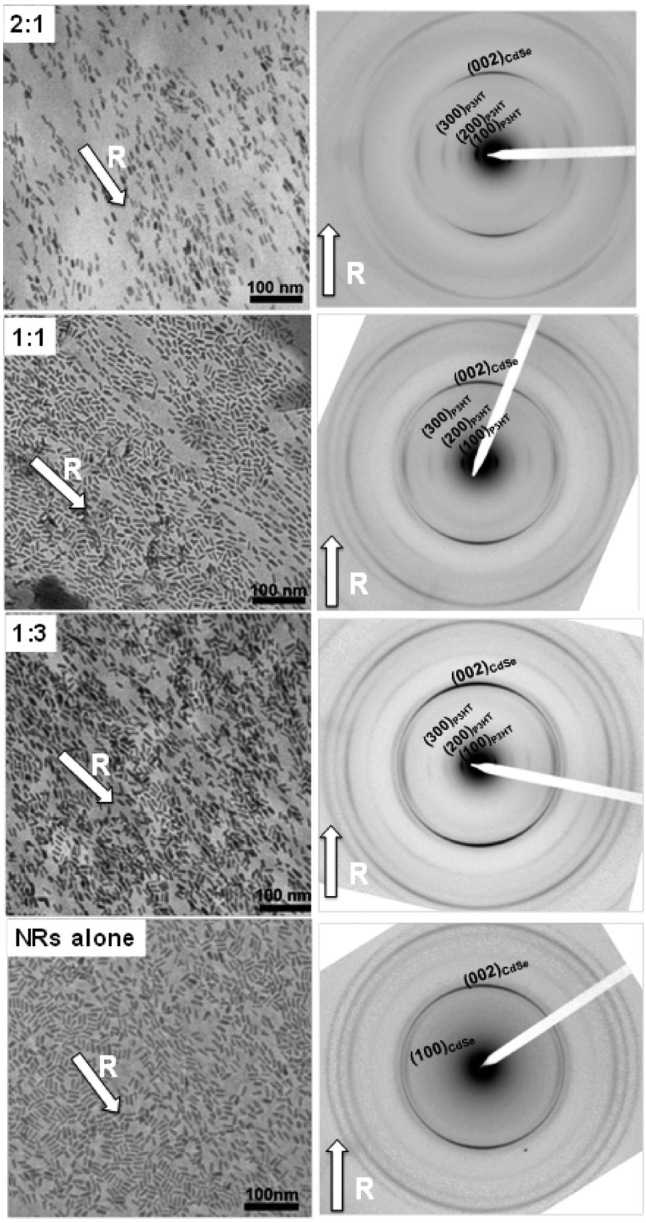

Figure 7. Evolution of the TEM-BF and corresponding ED patterns of hybrid P3HT:CdSe thin films as a function of increasing concentration of CdSe NRs. The rubbing direction **R** is indicated by an arrow. For the sake of comparison, a film of rubbed CdSe NRs is also displayed.

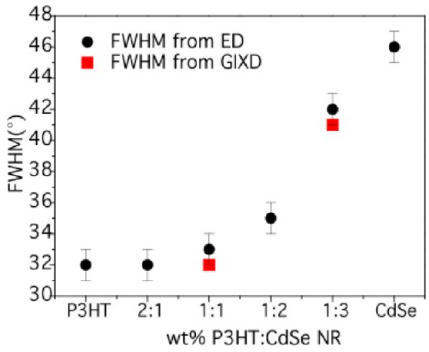

Figure 8. Full circles: fwhm of the azimuthal distribution extracted from the ED patterns of the $(002)_{CdSe}$ reflection. Red squares: fwhm extracted from GIXD Ω-scans of the $(002)_{CdSe}$ reflection.

Further evidence for a progressive loss of alignment of CdSe and P3HT in the films with increasing CdSe concentration is manifested by the evolution of the GIXD line profiles for $\mathbf{q}\|\mathbf{R}$, i.e., when the scattering vector **q** is directed along the long axis of NRs. As seen in Figure 9, while only the $(0\ 0\ 2)_{CdSe}$ diffraction line is obtained in the 1:1 sample, additional $(100)_{CdSe}$ and $(101)_{CdSe}$ reflections are observed for the 1:3 sample. These additional reflections indicate the presence of nonaligned CdSe NRs in the 1:3 sample, whereas most CdSe NRs were aligned with $\mathbf{c}_{CdSe}\|\mathbf{R}$ in the 1:1 sample.

Taken all together, these results evidence the concomitant decrease of the in-plane orientation of both CdSe NRs and P3HT chains when the concentration of NRs increases. In the light of HR-TEM and ED results, this trend suggests strongly that the alignment of CdSe NRs in the rubbed films is via the alignment of the polymer matrix, similarly to what occurs in stretch-oriented polymer nanocomposites although some direct alignment of CdSe NRs by rubbing may also occur.[23,27] However, the efficiency of NR alignment by the polymer is certainly conditioned by the interaction between the brush of

dx.doi.org/10.1021/ma400880x | Macromolecules 2013, 46, 6177−6186

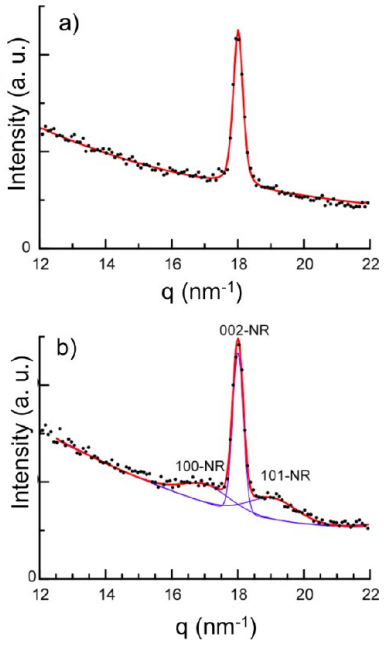

Figure 9. In-plane GIXD profiles obtained with **q**||**R** (c_{P3HT}) of (a) 1:1 and (b) 1:3 rubbed P3HT/CdSe film. The full lines correspond to the fits of the peak with either a single component for the 1:1 sample or the sum of three contributions for the 1:3 sample.

alkyl chains on the NRs and the *n*-hexyl side chains of P3HT. It can be anticipated that the presence of long alkyl chains grafted on the surface of the CdSe NRs favors both the NR dispersion in the P3HT matrix and the alignment of the NRs by the P3HT matrix during the rubbing process. An interesting finding in the present study is that both the orientation of the polymer matrix and the NRs decrease when the NR concentration increases. This means that the presence of CdSe NRs in the polymer matrix hampers the orientation of the P3HT chains by rubbing. One possible origin for this behavior is that a high CdSe NR concentration affects the semicrystalline structure of the P3HT films, presumably by reducing the dimensions of P3HT nanocrystals. Considering the average nanocrystal dimension extracted from the fwhm of the $(100)_{P3HT}$ reflection using the Scherrer formula, it indeed decreases from 16.4 to 13.2 nm when going from the 1:1 to the 1:3 samples. At the same time, it is not ruled out that when the NRs concentration in the P3HT matrix is increased, the NR tendency to assemble to form larger raft-like structures also increases. Recently, Composto and co-workers have demonstrated that gold NRs in a PMMA matrix are dispersed in the form of isolated NRs at low concentration and tend progressively to form discrete aggregates as their concentration in the film increases.[49] The bundling of NRs has been described experimentally and predicted theoretically.[49,50] Korgel et al. have shown that attractive dipole−dipole forces and van der Waals interactions favor the side-by-side association of NRs.[50] In the peculiar case of alignment via mechanical rubbing, the type of dispersion of the NRs in the polymer matrix, e.g., isolated NRs versus bundles, will be of utmost importance for the efficiency of orientation by rubbing. If orientation of the NRs occurs via the polymer matrix, then it will be most efficient if the NRs are dispersed individually in the polymer matrix. However, if NRs are present in the form of extended rafts, then one can expect a much more difficult alignment by the polymer matrix. Indeed, reorientation of NRs forming bundles of parallel aligned NRs implies either to disrupt the favorable interactions between NRs or to collectively reorient a bundle of NRs. Moreover, the bulk redistribution of CdSe NRs suggested by TEM tomography will certainly also be hampered by the presence of CdSe NRs aggregates. Clearly, both these cases make NR alignment more difficult, explaining in part the lower overall alignment observed at higher NR concentrations. Conversely, one can assume that the presence of large bundles of NRs interacting strongly together will also decrease the alignment efficiency of the surrounding P3HT chains.

V. CONCLUSION

Mechanical rubbing can be applied to hybrid materials in which the polymer and the inorganic component display a high level of in-plane orientation. Mechanical rubbing allows for the fabrication of hybrid films where the polymer chain axis direction (c_{P3HT}) and the long axis of the NRs (c_{CdSe}) align parallel to the rubbing direction. While the crystalline P3HT domains show a preferential "face-on" orientation, i.e., a (010) contact plane, CdSe NRs tend also to adopt a preferential (a, c) contact plane on the substrate (see Figure 10). Analysis of the orientation distribution of both CdSe NRs and P3HT chains in the plane of the substrate indicates that NRs alignment is due to a large extent to the orientation of the polymer matrix during rubbing. TEM Tomography suggests that CdSe NRs are redistributed from the bulk of the hybrid film toward the film/substrate interface. The overall level of orientation achieved by rubbing in hybrid films depends strongly on the concentration of CdSe NRs in the polymer matrix. With increasing ratio of NRs in the thin films, the degree of in-plane orientation decreases and tends toward that of a rubbed pure CdSe NRs film. The progressive decrease of in-plane orientation with increasing concentration of NRs is attributed to the larger difficulty to reorient bundles of NRs contrary to individually dispersed NRs. Mechanical rubbing is a simple method to obtain rapidly large areas (~cm^2) of highly oriented hybrid thin films where both the organic and the polymeric phase present a high degree of in-plane orientation for a given range of NRs concentration. Recent findings on large scale alignment of poly(2,5-bis(3-dodecyl-2-yl)thieno[3,2-*b*]thiophene) (C12-pBTTT) via high-temperature rubbing suggest that this method

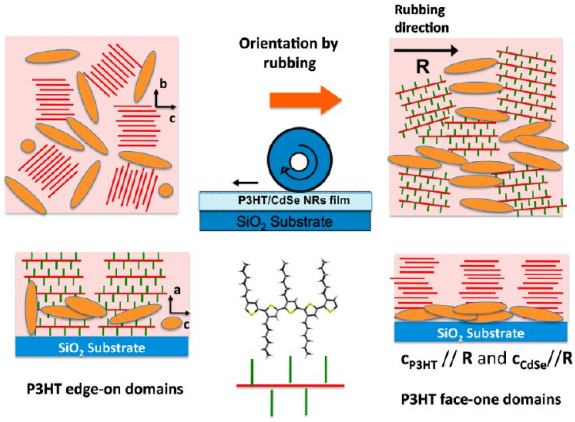

Figure 10. Schematic illustration of the orientation achieved via mechanical rubbing in hybrid thin films of P3HT and CdSe NRs: upper and lower images correspond to the top view and the section of the film morphology, respectively. For clarity, the P3HT chain segments of the amorphous phase are not shown.

dx.doi.org/10.1021/ma400880x | *Macromolecules* 2013, 46, 6177−6186

can potentially be applied to a large variety of hybrid polymer nanocomposites to generate and exploit original anisotropic optical, electric, and optoelectronic properties of functional hybrid films.[51]

■ ASSOCIATED CONTENT

Supporting Information

Absorption and fluorescence of CdSe NRs (Figure S0); bright field and ED patterns of rubbed CdSe NR films (Figure S1); table of experimental d_{hkl} values of CdSe NRs with calculated values using the wurtzite structure of CdSe; ED pattern and dark field image of a rubbed P3HT/CdSe (1:1 wt) film (Figure S2); UV−vis absorption spectra for parallel and perpendicular orientation of the rubbing direction to the incident light polarization and evolution of dichroic ratio with CdSe concentration (Figure S3). This material is available free of charge via the Internet at http://pubs.acs.org.

■ AUTHOR INFORMATION

Corresponding Author

*E-mail: martin.brinkmann@ics-cnrs.u-strasbg.fr (M.B.).

Present Address

[#]L.H.: Laboratoire des Matériaux Macromoléculaires et Organiques, STI/IMX, Station 12, EPFL, 1015 Lausanne, Switzerland.

Notes

The authors declare no competing financial interest.

■ ACKNOWLEDGMENTS

This work has been supported by the French National Agency (ANR) in the frame of its program in Nanosciences and Nanotechnologies (MYOSOTIS project no. ANR-08-NANO-012-01). L. Hartmann acknowledges financial support from the Région Alsace. ANKA and ESRF are gratefully acknowledged for beam time allocation.

■ REFERENCES

(1) Huynh, W. U.; Dittmer, J. J.; Alivisatos, A. P. *Science* **2002**, *295*, 2425−7.

(2) Aleshin, A. N.; Shcherbakov, I. P.; Petrov, V. N.; Titkov, A. N. *Org. Electron.* **2011**, *12*, 1285−1292.

(3) Zhang, R.; Li, B.; Iovu, M. C.; Jeffries-El, M.; Sauvé, G.; Cooper, J.; Jia, S.; Tristram-Nagle, S.; Smilgies, D. M.; Lambeth, D. N.; McCullough, R. D.; Kowalewski, T. *J. Am. Chem. Soc.* **2006**, *128*, 3480−1.

(4) Dayal, S.; Reese, M. O.; Ferguson, A. J.; Ginley, D. S.; Rumbles, G.; Kopidakis, N. *Adv. Funct. Mater.* **2010**, *20*, 2629−2635.

(5) Reiss, P.; Couderc, E.; De Girolamo, J.; Pron, A. *Nanoscale* **2010**, *3*, 446−489.

(6) (a) Beek, W. J. E.; Slooff, L. H.; Wienk, M. M.; Kroon, J. M.; Janssen, R. a. J. *Adv. Funct. Mater.* **2005**, *15*, 1703−1707. (b) Jiu, T.; Reiss, P.; de Bettignies, R.; Bailly, S.; Chandezon, F. *IEEE J. Sel. Top. Quantum Electron.* **2010**, *16*, 1619.

(7) Rauch, T.; Böberl, M.; Tedde, S. F.; Furst, J.; Kovalenko, M. V.; Hesser, G.; Lemmer, U.; Heiss, W.; Hayden, O. *Nat. Photonics* **2009**, *3*, 332−336.

(8) (a) Hartmann, L.; Tremel, K.; Uttiya, S.; Crossland, E.; Ludwigs, S.; Kayunkid, N.; Vergnat, C.; Brinkmann, M. *Adv. Funct. Mater.* **2011**, *21*, 4047−4057. (b) Jimison, L. H.; Toney, M. F.; McCulloch, I.; Heeney, M.; Salleo, A. *Adv. Mater.* **2009**, *21*, 1568.

(9) Persano, A.; De Giorgi, M.; Fiore, A.; Cingolani, R.; Manna, L.; Cola, A.; Krahne, R. *ACS Nano* **2010**, *4*, 1646−52.

(10) Evans, B. A.; Shields, A. R.; Carroll, R. L.; Washburn, S.; Falvo, M. R.; Superfine, R. *Nano Lett.* **2007**, *7*, 1428−34.

(11) Ryan, K. M.; Mastroianni, A.; Stancil, K. A.; Liu, H.; Alivisatos, A. P. *Nano Lett.* **2006**, *6*, 1479−82.

(12) Li, L.; Walda, J.; Manna, L.; Alivisatos, A. P. *Nano Lett.* **2002**, *2*, 557−560.

(13) Talapin, D. V.; Lee, J.-S.; Kovalenko, M. V.; Shevchenko, E. V. *Chem. Rev.* **2010**, *110*, 389−458.

(14) Ghezelbash, A.; Koo, B.; Korgel, B. A. *Nano Lett.* **2006**, *6*, 1832−6.

(15) Sun, B.; Sirringhaus, H. *J. Am. Chem. Soc.* **2006**, *128*, 16231−7.

(16) Baker, J. L.; Widmer-Cooper, A.; Toney, M. F.; Geissler, P. L.; Alivisatos, A. P. *Nano Lett.* **2010**, *10*, 195−201.

(17) Hung, A. M.; Konopliv, N. A.; Cha, J. N. *Langmuir* **2011**, *27*, 12322−8.

(18) Rivest, J. B.; Swisher, S. L.; Fong, L.-K.; Zheng, H.; Alivisatos, A. P. *ACS Nano* **2011**, *5*, 3811−6.

(19) Modestino, M. A.; Chan, E. R.; Hexemer, A.; Urban, J. J.; Segalman, R. A. *Macromolecules* **2011**, *44*, 7364−7371.

(20) Gupta, S.; Zhang, Q.; Emrick, T.; Russell, T. P. *Nano Lett.* **2006**, *6*, 2066−9.

(21) Breiby, D. W.; Chin, P. T. K.; Andreasen, J. W.; Grimsrud, K. A.; Di, Z.; Janssen, R. A. J. *Langmuir* **2009**, *25*, 10970−4.

(22) Chin, P. T. K.; Hikmet, R. A. M.; Meskers, S. C. J.; Janssen, R. A. J. *Adv. Funct. Mater.* **2007**, *17*, 3829−3835.

(23) Hikmet, R. A. M.; Chin, P. T. K.; Talapin, D. V.; Weller, H. *Adv. Mater.* **2005**, *17*, 1436−1439.

(24) Amit, Y.; Faust, A.; Lieberman, I.; Yedidya, L.; Banin, U. *Phys. Status Solidi A* **2012**, *209*, 229.

(25) Van der Zande, B. M. I.; Pagès, L.; Hikmet, R. A. M.; Van Blaaderen, A. *J. Phys. Chem. B* **1999**, *103*, 5761−5767.

(26) Al-Rawashdeh, N. A. F.; Sandrock, M. L.; Seugling, C. J.; Foss, C. A. *J. Phys. Chem. B* **1998**, *102*, 361−371.

(27) Murphy, C. J.; Orendorff, C. J. *Adv. Mater.* **2005**, *17*, 2173−2177.

(28) Murphy, C. J.; Sau, T. K.; Gole, A. M.; Orendorff, C. J.; Gao, J.; Gou, L.; Hunyadi, S. E.; Li, T. *J. Phys. Chem. B* **2005**, *109*, 13857−70.

(29) Rizzo, A.; Mazzeo, M.; Palumbo, M.; Lerario, G.; D'Amone, S.; Cingolani, R.; Gigli, G. *Adv. Mater.* **2008**, *20*, 1886−1891.

(30) Rizzo, A.; Nobile, C.; Mazzeo, M.; De Giorgi, M.; Fiore, A.; Carbone, L.; Cingolani, R.; Manna, L.; Gigli, G. *ACS Nano* **2009**, *3*, 1506−12.

(31) Brinkmann, M. *J. Polym. Sci., Part B: Polym. Phys.* **2011**, *49*, 1218−1233.

(32) O'Connor, B.; Kline, R. J.; Conrad, B. R.; Richter, L. J.; Gundlach, D.; Toney, M. F.; DeLongchamp, D. M. *Adv. Funct. Mater.* **2011**, *21*, 3697−3705.

(33) Brinkmann, M.; Wittmann, J.-C. *Adv. Mater.* **2006**, *18*, 860−863.

(34) Brinkmann, M.; Aldakov, D.; Chandezon, F. *Adv. Mater.* **2007**, *19*, 3819−3823.

(35) Schierhorn, M.; Boettcher, S. W.; Peet, J. H.; Matioli, E.; Bazan, G. C.; Stucky, G. D.; Moskovits, M. *ACS Nano* **2010**, *4*, 6132−6136.

(36) Snaith, H. J.; Whiting, G. L.; Sun, B.; Greenham, N. C.; Huck, W. T. S.; Friend, R. H. *Nano Lett.* **2005**, *5*, 1653−7.

(37) Toney, M. F.; Russell, T. P.; Logan, J. A.; Kikuchi, H.; Sands, J. M.; Kumar, S. K. *Nature* **1995**, *374*, 709.

(38) (a) Brinkmann, M.; Pratontep, S.; Chaumont, C.; Wittmann, J.-C. *Macromolecules* **2007**, *40*, 9420−9426. (b) Vergnat, C.; Uttiya, S.; Pratontep, S.; Kerdcharoen, T.; Legrand, J.-F.; Brinkmann, M. *Synth. Met.* **2011**, *161*, 251. (d) Vergnat, C.; Landais, V.; Legrand, J.-F.; Brinkmann, M. *Macromolecules* **2011**, *44*, 3817−3827. (e) Vergnat, C.; Landais, V.; Combet, J.; Vorobiev, A.; Konovalov, O.; Legrand, J.-F.; Brinkmann, M. *Org. Electron.* **2012**, *13*, 1594.

(39) Talapin, D. V.; Nelson, J. H.; Shevchenko, E. V.; Aloni, S.; Sadtler, B.; Alivisatos, A. P. *Nano Lett.* **2007**, *7*, 2951−9.

(40) Carbone, L.; Nobile, C.; De Giorgi, M.; Sala, F. D.; Morello, G.; Pompa, P.; Hytch, M.; Snoeck, E.; Fiore, A.; Franchini, I. R.; Nadasan, M.; Silvestre, A. F.; Chiodo, L.; Kudera, S.; Cingolani, R.; Krahne, R.; Manna, L. *Nano Lett.* **2007**, *7*, 2942−50.

(41) Saxton, W.; Baumeister, W.; Hahn, M. *Ultramicroscopy* **1984**, *13*, 57−70.

(42) Mastronarde, D. N. *J. Struct. Biol.* **1997**, *120*, 343−352.
(43) Gordon, R.; Bender, R.; Herman, G. T. *J. Theor. Biol.* **1970**, *24*, 471−481.
(44) Midgley, P. A.; Weyland, M. *Ultramicroscopy* **2003**, *96*, 413.
(45) Florea, I.; Ersen, O.; Hirlimann, C.; et al. *Nanoscale* **2010**, *2* (12), 2668−2678.
(46) Roiban, L.; Hartmann, L.; Fiore, A.; Djurado, D.; Chandezon, F.; Reiss, P.; Legrand, J.-F.; Doyle, S.; Brinkmann, M.; Ersen, O. *Nanoscale* **2012**, *4*, 7212.
(47) McBride, J. R.; Kippeny, T. C.; Pennycook, S. J.; Rosenthal, S. J. *Nano Lett.* **2004**, *4*, 1279.
(48) (a) Brinkmann, M.; Rannou, P. *Macromolecules* **2009**, *42*, 1125. (b) Salammal, T. S.; Mikayelyan, E.; Grigorian, S.; Pietsch, U.; Koenen, N.; Scherf, U.; Kayunkid, N.; Brinkmann, M. *Macromolecules* **2012**, *45*, 5575.
(49) (a) Jiang, G.; Hore, M. J. A.; Gam, S.; Composto, R. J. *ACS Nano* **2012**, *6*, 1578. (b) Hore, M. J. A.; Composto, R. J. *ACS Nano* **2010**, 6941.
(50) Ghezelbash, A.; Koo, B.; Korgel, B. A. *Nano Lett.* **2006**, *6*, 1832.
(51) Biniek, L.; Leclerc, N.; Heiser, T.; Bechara, R.; Brinkmann, M. *Macromolecules* **2013**, *46*, 4014.